Article

Metal Release and Cell Viability of 316L Stainless Steel Sputter-Coated with N-Doped a-C:H Coatings

António Fróis [1,2,3], João Ricardo Marques [2], Luís Santos [4], Marco Peres [5,6,7], Katharina Lorenz [5,6,7], Cristina Santos Louro [1] and Ana Cristina Santos [1,2,3,*]

[1] Department of Mechanical Engineering, CEMMPRE, ARISE, University of Coimbra, Rua Luis Reis Santos, 3030-177 Coimbra, Portugal; antonio.frois@student.uc.pt (A.F.); cristina.louro@dem.uc.pt (C.S.L.)
[2] Faculty of Medicine, Biophysics Institute, Coimbra Institute for Clinical and Biomedical Research/Centre for Innovative Biomedicine and Biotechnology (iCBR/cibb), University of Coimbra, 3000-548 Coimbra, Portugal; jrmm@student.uc.pt
[3] Faculty of Medicine, Center for Research in Environment, Genetics and Oncobiology (CIMAGO), University of Coimbra, 3000-548 Coimbra, Portugal
[4] Centro de Química Estrutural, Departamento de Engenharia Química, Institute of Molecular Sciences, Instituto Superior Técnico (IST), University of Lisbon, Av. Rovisco Pais, 1049-001 Lisboa, Portugal; luis.santos@tecnico.ulisboa.pt
[5] IPFN, Instituto Superior Técnico (IST), Campus Tecnológico e Nuclear, Estrada Nacional 10, 2695-066 Bobadela, Portugal; marcoperes@ctn.tecnico.ulisboa.pt (M.P.); lorenz@ctn.tecnico.ulisboa.pt (K.L.)
[6] Instituto de Engenharia de Sistemas e Computadores-Microsistemas e Nanotecnologia (INESC-MN), Rua Alves Redol 9, 1000-029 Lisboa, Portugal
[7] DECN, Instituto Superior Técnico, University of Lisbon, 2695-066 Bobadela, Portugal
* Correspondence: acsantos@fmed.uc.pt

Featured Application: This research work demonstrates that undoped a-C:H sputtered coatings can effectively inhibit the metallic release from medical-grade 316L stainless steel in acidic artificial saliva without a significant change in the microstructural characteristics. Moreover, the in vitro biocompatibility with macrophages and/or fibroblasts was significantly improved. In opposition, the a-C:H:N system seems to be unfavorable, even for low N content up to 10 at.%.

Abstract: Hydrogenated amorphous carbon (a-C:H) has been considered a promising biocompatible coating to protect metallic alloys against corrosion for medical applications, namely orthodontics. However, there is still no optimal solution for this biomedical field; hence, the investigation remains open. In this work, the effect of a nonmetallic doping element (N) on sputter-deposited a-C:H coatings was studied concerning both salivary corrosion and cytotoxicity behavior. After a 30-day corrosion test in an acidic modified Fusayama-Meyer artificial saliva, metal release from both coated and uncoated 316L stainless steel (SS) substrates was quantified. Tests on the corrosion extracts were then performed by using monocultures of macrophages and fibroblasts, and their coculture; and cell viability was evaluated via the MTT test. Results show an overall inhibition of the SS corrosion, which enhanced the in vitro biocompatibility with a minimal effect on the coatings' microstructure. Among all the coatings tested, the undoped a-C:H coating performed the best, whereas an increase in N doping led to poorer protection against metal dissolution and a subsequent slightly lower biocompatibility. The findings corroborate that selecting the nonmetallic element N for doping C-based coatings is not a good choice for this biomedical field, even at low contents up to 10 at.%.

Keywords: cytotoxicity; corrosion; DLC coatings; hydrogenated amorphous carbon (a-C:H); metal release; nitrogen doping; orthodontics; protective coatings; sputtering

1. Introduction

Any metallic alloy ultimately corrodes in vivo [1,2], namely inside the human mouth. However, the first-generation biomaterials are still widely used in applications that require

demanding mechanical properties, such as orthodontics. Stainless steel (SS), titanium (Ti) and its alloys, and cobalt (Co)-chromium (Cr) alloys are typical representative biometals in the referred medical field, providing the required load to induce tooth movement for correcting malocclusions [3,4].

Despite the alloys' biocompatibility—basic criteria for any material to be considered a biomaterial—concerns have been intensified regarding the effects of the intraoral environment in promoting metallic corrosion, which is ultimately accompanied by the release of metallic ions. Some of those ions—such as Ni(II)—cause allergic reactions and can be toxic to cells and tissues [2,5,6]. Therefore, further research is required to functionalize these bioalloys, while taking advantage of the already suitable bulk mechanical properties. Among the several surface treatments, coating deposition techniques, and classes of materials reported in the literature—for medical and biotechnological applications and orthodontics in particular [4,7]—the potential of the amorphous C-based coatings deposited by sputtering must be highlighted.

Physical vapor deposition (PVD) methods—including sputtering—present several advantages for demanding functional medical applications: it enables the deposition from monolithic to composite materials and equilibrium to metastable structures; it yields high deposition rates; and sputtered coatings exhibit better adhesion compared to others deposited by other methods, namely high purity, ecofriendliness, uniformity, and high reproducibility [8,9]. Moreover, H-free and hydrogenated amorphous carbon coatings (a-C and a-C:H, respectively), including the so-called Diamond-Like Carbon (DLC), can be deposited by sputtering and are well-established due to their chemical inertness, and overall biocompatibility [10].

Following the same approach that has long been used for the development of protective coatings in the mechanical and tribological fields, doping of DLCs with metals and nonmetals has been a common method for bioapplications [11,12]. Moreover, for certain doping concentration ranges, the amorphous structure of DLC coatings can be preserved, therefore avoiding certain defects of the crystalline networks, such as grain boundaries, that are favored sites for phase precipitation and chemical reactions—such as corrosion. This has been explored recently by the authors, namely by selecting a less used element—nitrogen (N)—as a dopant of the a-C:H coatings produced by sputtering. The findings concerning the bacterial adhesion inhibition corroborate that the best N doping level was 6 at.% [13].

The main objective of the current research is to understand whether the reactively sputtered a-C:H:N coatings can fulfill the trinomial saliva physicochemical parameters—living tissues—plaque-forming micro-organisms, that characterize the complex oral cavity environment. Aiming at orthodontics, it is intended to complete the study of the C-H-N system onto medical-grade 316L SS, preserving the N concentration up to 10 at.%. For that purpose, in vitro aggressive parameters were selected to better mimic the human mouth. The purpose of this article is twofold: (i) to assess the corrosion behavior of both uncoated and DLC-coated 316L SS substrates; and (ii) to evaluate the resulting in vitro cytotoxicity of their respective eluates in artificial saliva, using monocultures of macrophages and fibroblasts and their coculture.

2. Materials and Methods

2.1. Coatings Deposition

The deposition process of the a-C:H:N coatings onto 316L SS (AISI) substrates by reactive d.c. magnetron sputtering was performed in a system equipped with two cathodes (graphite and titanium, 99.9% purity), as previously described elsewhere [13]. Briefly, previously polished square-shaped ($10 \times 10 \times 2$ mm) SS substrates were etched by Ar bombardment, followed by the deposition of a Ti-based interlayer. Finally, three different top C-based top layers were synthesized by varying the reactive N_2 flow for a fixed CH_4/Ar flow ratio. The coatings will be identified according to their dopant content: the reference undoped CH_0N and the doped CH_6N and CH_9N, as summarized in Table 1.

Table 1. Main characteristics of the as-deposited coatings.

Coating	Relative N_2 Flow [1] [%]	Thickness [nm]		N Content [at.%]		H Content [at.%]
		Ti Interlayer	C Top Layer	(XPS [1])	(EDS)	(ERDA [1])
CH_0N	0	366	801	—	—	33
CH_6N	7.9	349	820	5.6	6.5	27
CH_9N	12.5	361	928	9.0	9.4	25

[1] Values reproduced from [13].

2.2. Coatings Characterization

The surface and cross-section morphology of the deposited coatings, as well as thickness measurements, were assessed by high-resolution field-emission Scanning Electron Microscopy (SEM) by using a ZEISS Merlin Compact/VP Compact equipment. The cross-section elemental distribution maps were obtained by using an Energy Dispersive Spectroscopy (EDS) detector (X-Max Oxford Instruments, Oxford, UK) coupled to the SEM system.

The evolution of the structure and chemical bonding of the coatings upon immersion was studied through visible Raman in a LabRAM HR 800 Evolution spectrometer (Horiba, Vénissieux, France), equipped with a 532 nm external laser source and coupled with an Olympus BXFM confocal microscope ($100\times$ objective, yielding a spot size of ~1 μm, and a power of ~10 mW at the sample). The Raman spectra were curve-fitted into two main Gaussian functions after linear background subtraction, corresponding to the D and G characteristic bands of amorphous carbon materials [14,15].

Prior to wettability analysis, all samples were ultrasonically cleaned in ethanol and distilled water, sequentially. The static water contact angles (WCA) were measured with distilled water drops (4 μL/s) in a CAM100 equipment (KSV Instruments Ltd., Helsinki, Finland). A minimum of four measurements per sample was performed.

The coating's surface topography was assessed by Atomic Force Microscopy (AFM), by acquiring 3D images and calculating the average roughness (Ra) in a Veeco DiInnova equipment running in intermittent mode (4×4 μm^2 area).

2.3. Metal Release in Artificial Saliva

Static corrosion tests were performed by immersing the samples in an acidic (pH = 2.3) modified Fusayama-Meyer artificial saliva bath in sterile conditions for 30 days at, 37 °C, by adapting the ISO 10271 protocol [16]. A surface-to-area ratio of 1 cm^2/10 mL was preserved [17,18]. The chemical composition of the artificial saliva was the following: KCl—0.4 g/L; NaCl—0.4 g/L; $CaCl_2 \bullet 2H_2O$—0.906 g/L; $NaH_2PO_4 \bullet 2H_2O$—0.69 g/L; $Na_2S \bullet 9H_2O$—0.005 g/L; and HCl (1M)—until pH = 2.3. Samples were previously sterilized by UV radiation (30 min per side), whereas the artificial saliva was autoclaved (Uniclave 77, AJC, Cacém, Portugal). At the end of the immersion test, the solutions—hereby termed "corrosion extracts"—were retrieved for further analysis. The metallic elements (Ni, Cr, and Fe) in solution were quantified, in triplicate, by Inductively Coupled Plasma—Optical Emission Spectroscopy (ICP-OES) in a Horiba Jobin-Yvon Ultima apparatus (Edison, NJ, USA). The average metal release rates for each element, per day and per surface area, were then calculated. The ICP-OES detection limits for Cr, Fe, and Ni were 1.18, 1.48, and 3.73 μg/L, respectively.

2.4. Cytotoxicity Tests
2.4.1. Cell Cultures

In this work, two types of cells were used to assess the cytotoxicity of the corrosion extracts: the NIH/373 (ATCC® CRL-1658™, American Type Culture Collection (Manassas, VA, USA)) fibroblasts [19]; and fresh macrophages (primary culture) from Wistar rats (*Rattus norvegicus albinus*), collected in-house according to the protocol described [20]. Both cell types were incubated using Dulbecco's Modified Eagle's Medium (DMEM, Gibco® 1×,

11966-025, ThermoFisher Scientific, Altrincham, UK) supplemented with 5% fetal bovine serum (FBS, Sigma-Aldrich®, F7524, St. Louis, MO, USA), 1% L-glutamine (L-Glutamine 100×, 200 mM, XO55O-100, Biowest, Nuaillé, France), and 1% antibiotics (penicillin and streptomycin, Lonza Pen Srep, Amphotericin, B 100×, 17-745, Lonza Walkersville Inc., Walkersville, MD, USA) at 37 °C, 5% CO_2, and 95% humidity (Binder incubator, CB 150, Uster, Switzerland).

2.4.2. Testing of the Extracts

Prior to the in vitro tests, the corrosion extracts retrieved from the corrosion tests (see Section 2.3) were filtered twice using FP 30/0.2 μL filters (10462200, Whatman, OH, USA) to prevent any culture contamination. According to ISO 10993-5 [21] and by adapting the protocol developed and followed by Costa et al. [22], fibroblasts were then seeded separately or as coculture in 48-well flat-bottom plates (Corning Inc. Costar®, 3548, Corning, NY, USA) in sterile conditions (flow laminar chamber, Heraeus Holten, HBB 2448, LabExchange, Germany). A total number of 2.6×10^3 fibroblasts and/or 5×10^4 macrophages per well were used. For controls, 600 μL of culture medium was added to each well; for testing the extracts, 67 μL of each corrosion extract or artificial saliva was used to attain the same total volume, completed with DMEM 5%. Plates were prepared to be incubated for 5 days (macrophages monoculture) or 6 days (fibroblast monoculture or coculture with macrophages) under standard conditions (37 °C, 5% CO_2, 95% humidity). At least 3 independent assays were performed for each culture type.

2.4.3. MTT Test

At the end of the incubation periods, cell viability was quantified by the MTT (3-[4,5-dimethylthiazol-2-yl]-2,5-diphenyltetrazolium bromide) assay [23]. After aseptically removing the content of each well, fresh culture medium (without FBS) and MTT at 10% were added (total volume of 450 μL). The plates were placed inside the incubator for 4 h in the described standard conditions. Afterwards, the solution of each well was replaced by 450 μL of acidic isopropanol to stabilize the formazan crystals for 15 min (at room temperature over the bench under light protection). Finally, the absorbance was measured at 570 nm with a reference filter of 620 nm using a spectrophotometer (Biotek Synergy HT, Winooski, VT, USA).

2.4.4. Statistical Analysis

The RStudio software [24] (version 4.2.3) was used to analyze the MTT results. Data from each well was standardized regarding its control and depicted as boxplot diagrams. The standardization line (SL, y = 1) was included as a reference, referring to the average value of the controls (100%). The 70% level (y = 0.7) is also included and can be understood as the limit that divides cytotoxic (>70%) and noncytotoxic materials (<70%) [25]. To perform the statistical analysis, the nonparametric Kruskal–Wallis test was first used to search for significant differences among the medians of the studied groups. The null hypothesis was that "there are no statistically significant differences between the studied groups", considering an α value of 0.05 (a confidence interval of 95%). If $p < \alpha$, the Mann–Whitney test was applied to assess for the statistically significant differences between 2 independent samples for the same confidence interval. The following notation is used in the boxplots for identifying the statistically significant differences: * $p < 0.05$; ** $p < 0.01$; and *** $p < 0.001$.

3. Results and Discussion

3.1. As-Deposited Characterization

To complement the as-deposited characterization of the sputtered a-C:H:N coatings previously reported [13], a new summary can be found in Table 1 for the coatings in the study.

Nitrogen quantification by EDS analysis revealed a doping range between 5 and 10 at.%, confirming previous XPS results (Table 1). The N content in the films increased with the reactive N_2 flow, associated with a decrease in hydrogen incorporation (from ~33 to 25 at.%), as quantified by Elastic Recoil Detection Analysis (ERDA) and Rutherford Backscattering Spectrometry (RBS). Moreover, both the previous XPS and Raman spectroscopy analysis corroborated a progressive graphitization of the C-based matrix upon doping, confirming that nitrogen promotes the formation of C=N bonds and enhances the total sp^2 hybridization of carbon in the sputtered a-C:H:N coatings.

Representative cross-section and surface SEM morphologies of the as-deposited undoped and doped coatings can be seen in Figure 1. A well-defined columnar layer with a thickness of approximately 360 nm characterizes the Ti-based adhesion-promoting interlayer, just below a contrasting thicker (800–900 nm) and dense top external layer (Table 1). Thus, doping with N does not seem to change the featureless morphology of the undoped a-C:H layer by using the selected sputtering conditions of this study, as shown in Figure 1b for the coating with the highest N content (CH_9N). Nevertheless, the typical surface conical defects [26] become rare, allowing the observation of a more "scratched"/"groove"-like morphology of the coating that followed the imperfect surface mechanical polishing of the SS surface. Even so, surface roughness was not significantly affected by the N doping effect (Ra between ~2.9 and 3.4 nm), accompanied by a decrease in the WCA from ~81 to 73° [13] (Figure 2a).

The EDS cross-section elemental distribution maps (Figure 1) confirm the architecture of the coatings under study. Immediately above the Si substrate, a strong Ti Kα signal, originated from the interlayer, was detected, followed by a wide carbon band due to the top layer. While carbon seems to be well distributed through the coatings' thickness, the nitrogen doping element appears to be more concentrated in the adhesion layer (Figure 1b). This nonhomogeneous distribution of nitrogen during film formation was expected. In fact, titanium has a higher affinity for nitrogen in comparison to carbon [ΔH^o_f (TiN) = -80.4 kcal/mol, ΔH^o_f (TiC) = -57 kcal/mol] [27]. Thus, when the coatings are deposited under an N_2-containing reactive atmosphere, preferential nitrogen interdiffusion can occur from the growing top C-based layer to the presputtered interlayer.

3.2. Corrosion Behavior

Static immersion tests are economic and simple methods for studying the corrosion behavior of materials for extended time periods, simulating as closely as possible what might happen in real-life situations, namely in orthodontics. After the 30-day immersion test in acidic artificial saliva with pH 2.3, no coating damages were identified.

As shown in Figure 2, the coatings' Ra systematically increased upon immersion (more than doubles), with more pronounced surface morphological features as seen in the 3D AFM topographic maps. Similarly, the wettability of the coatings increased, as seen by the opposite trend in the recorded WCA values (Figure 2), which may be justified by the variation of surface roughness. Indeed, and according to Wenzel's equation [28,29], if the surface is in the hydrophilic regime (WCA < 90°, which is the case of the coatings under study), an increase in surface roughness will lead to a decrease in the WCA, as previously reported [30]. Nonetheless, the undoped CH_0N was the most stable coating, while the doped CH_6N and CH_9N showed higher variations in the WCA. The corrosion-promoting environment can also foster the formation of oxygen-containing hydrophilic groups, accompanied by a reduction in the number of hydrocarbon groups [31], with a possible effect on the WCA of the aged coatings. Other more significant alterations, such as discoloration, detachment, or cracking detected by other researchers [32–34] were unnoticeable in the present study.

The C-bonding configuration of the coatings was evaluated by Raman analysis, Figure 3. As can be seen, Raman spectra of CH_0N and CH_6N coatings almost overlap, indicating that the immersion did not significantly affect its as-deposited C-bonding configurations, Figure 3a. The evolution of the Raman features upon curve fitting is summarized in Table 2

and depicted in Figure 3b, namely regarding the D and G peak positions—Pos(D) and Pos(G) –, and the intensity ratio between both bands—I_D/I_G. Nevertheless, results from the coating with the highest N content (CH_9N)—which was already the one with the highest as-deposited total sp^2/sp^3 content [13]—suggest that it underwent graphitization upon the 30-day immersion. This is noticeable in Figure 3b, where both Pos(G) and I_D/I_G ratio rise, being indicative of a less disorderly structure with an increase in the size and/or number of sp^2 clusters [14].
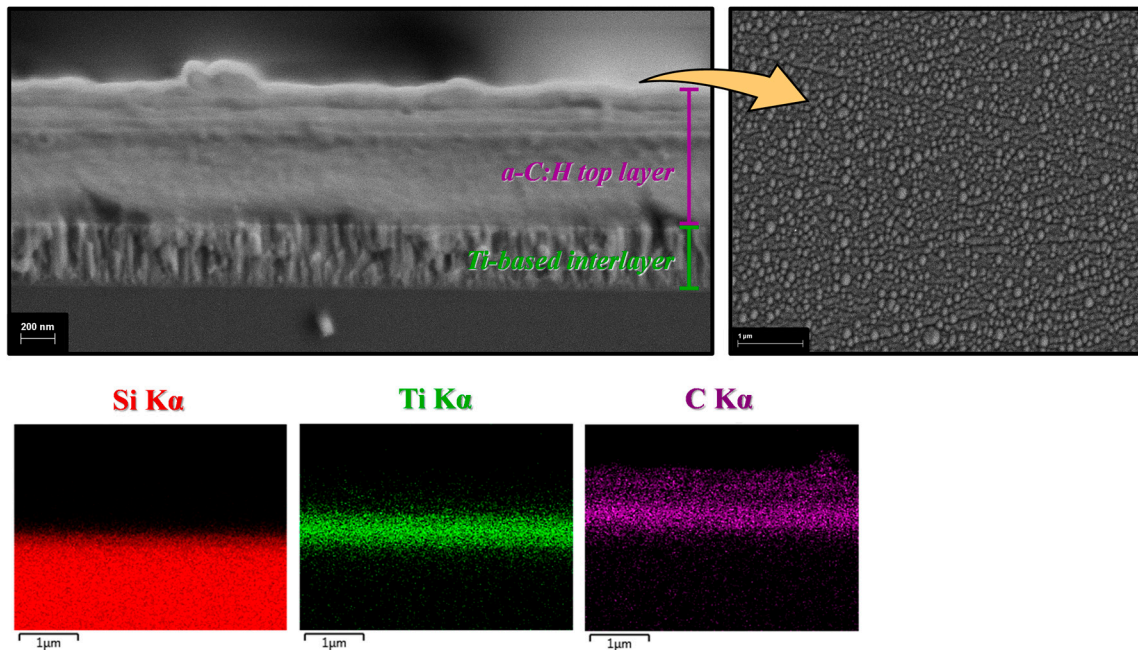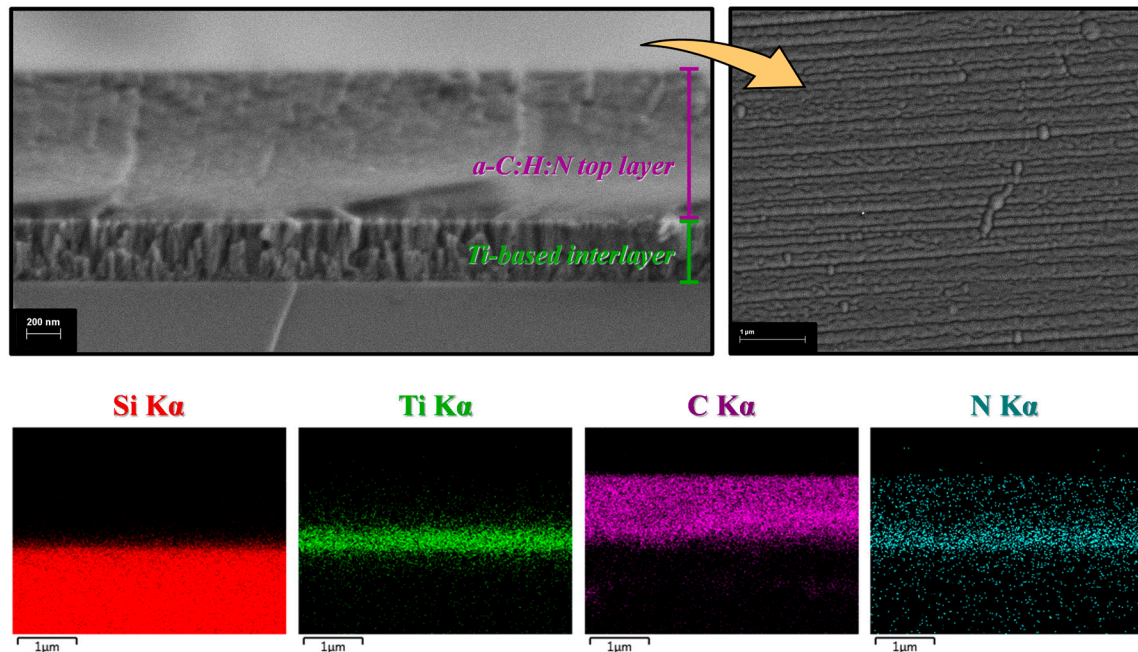

Figure 1. Cross-section and surface SEM micrographs coupled with the corresponding EDS elemental distribution maps of the as-deposited (**a**) CH_0N and (**b**) CH_9N coatings deposited onto Si substrates.
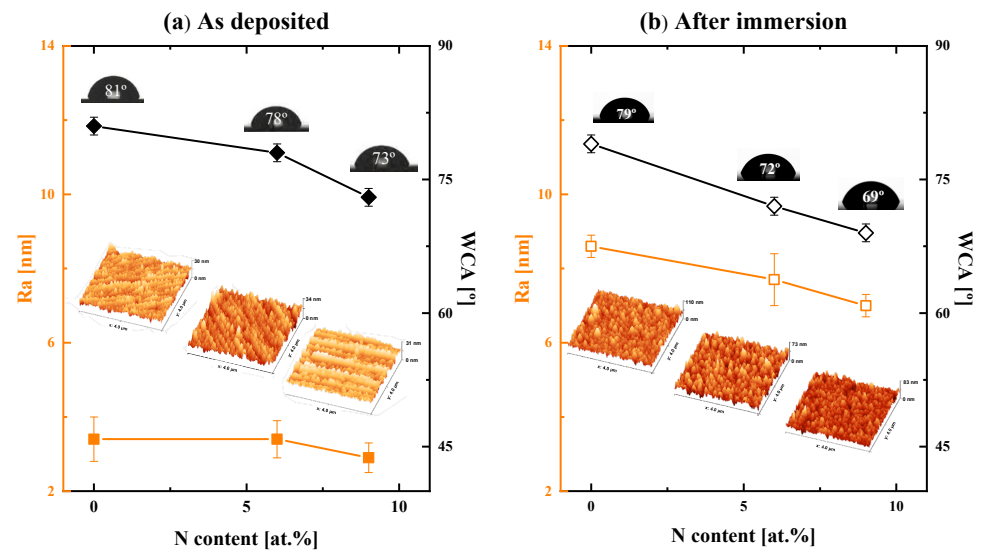
Figure 2. Evolution of the Ra and WCA with N doping content, for both (**a**) as deposited [13] and (**b**) post-immersion coatings, coupled with representative 3D AFM topographic maps ($4 \times 4 \ \mu m^2$) and optical image of droplets.

Table 2. Raman curve fitting parameters of the as-deposited and as-immersed coatings.

Coating	Condition	Pos(G)	Pos(D)	I_D/I_G
CH_0N	As-deposited	1552	1372	0.77
	As-immersed	1553	1374	0.76
CH_6N	As-deposited	1553	1378	0.89
	As-immersed	1553	1378	0.89
CH_9N	As-deposited	1560	1384	1.09
	As-immersed	1562	1385	1.15

The N-induced decrease in the sp^3 content, along with the higher surface hydrophilicity [35], may help in explaining the worse corrosion behavior of the doped films. The average release rates of the three main elements in the SS nominal composition—Ni, Cr, and Fe—are compiled in Figure 4.

The analysis of each metal in the solution revealed a substantial reduction in nickel and iron average release rates, by approximately 70%, for the steel substrates coated with undoped a-C:H, that is, CH_0N (Figure 4), while Cr release rate remained approximately constant. Accordingly, it is possible to conclude that the corrosion resistance of the medical-grade 316L SS in the acidic solution was improved by depositing the dense amorphous C-based coating with a Ti-based adhesion-promoting interlayer.

Other authors also reported a significant decrease in the commonly focused Ni element from several metallic alloys [36–40], with an overall biocompatibility enhancement, by using DLC protective coatings. Nonetheless, in a previous study concerning the protection of SS against corrosion by coating with a-C:H-based coatings, considerably higher Ni, Cr, and Fe release rates from coated substrates were found when compared with the bare SS ones [18]. Such disappointing and unexpected results evidenced the need to consider the substrate/coating system as a whole. Metallic-based interlayers can actually induce galvanic coupling effects at reactive interfaces within the coating [41], deteriorating the corrosion resistance of the alloy with a resulting increase in the concentration of metallic ions in the electrolyte. In the current work, the increase in the overall release rate seems to be related to the doping element itself, when compared to the undoped CH_0N one. In fact, for the coatings with up to ~9 at.% of N, more modest inhibition in the Ni release rates were achieved: only ~20% (Figure 4), contrasting with the previously mentioned 70% for the undoped film. Similarly, the Fe release rates seem to follow Ni's, whereas a slight increase

in Cr release was detected. Nitrogen addition clearly led to a lower corrosion inhibition ability of the DLC coating.
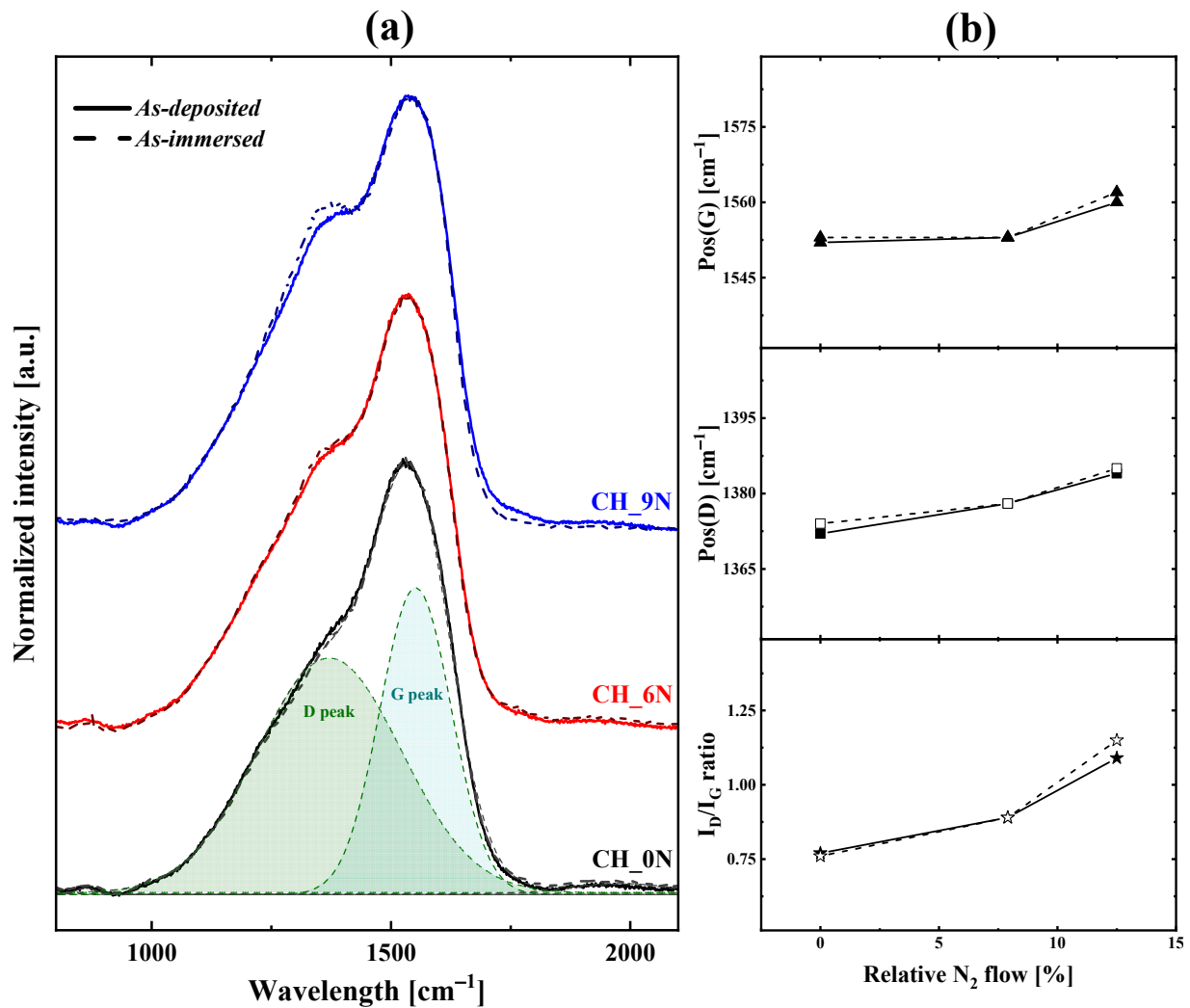

Figure 3. Raman results of the as-deposited and as-immersed coatings: (**a**) Raman spectra; and (**b**) obtained Pos(G), Pos(D), and I_D/I_G ratio upon curve fitting. A typical curve fitting for the as-deposited CH_0N coating into the G and D peaks is also presented.

According to the literature, N doping contents above ~10 at.% are expected to increase the electrical conductivity of the a-C:H:N material [14], which is a serious disadvantage for protective coatings operating in corrosive/oxidizing environments. In fact, coatings with ~11 at.% of N show improved electron transfer ability for redox reactions, which makes them suitable for other applications, such as biosensors [42]. However, for lower N contents, this effect has been reported to be minimal, and an improved corrosion resistance would be expected, by maintaining the threshold value of ~10 at.%. This motivated the selection of this non-metallic element as the dopant in the current work. Surprisingly, the results were beyond expectations. While for the CH_9N, a deleterious effect of the doping level might occur due to the proximity with the threshold value, the opposite should occur for the CH_6N, in accordance with its better bacterial adhesion inhibition properties [13].

Overall, the high corrosion resistance of the 316L SS alloy can be further optimized by deposition a top compact well-adherent a-C:H film, with a WCA close to 80° and a promoting Ti-based adhesion layer.
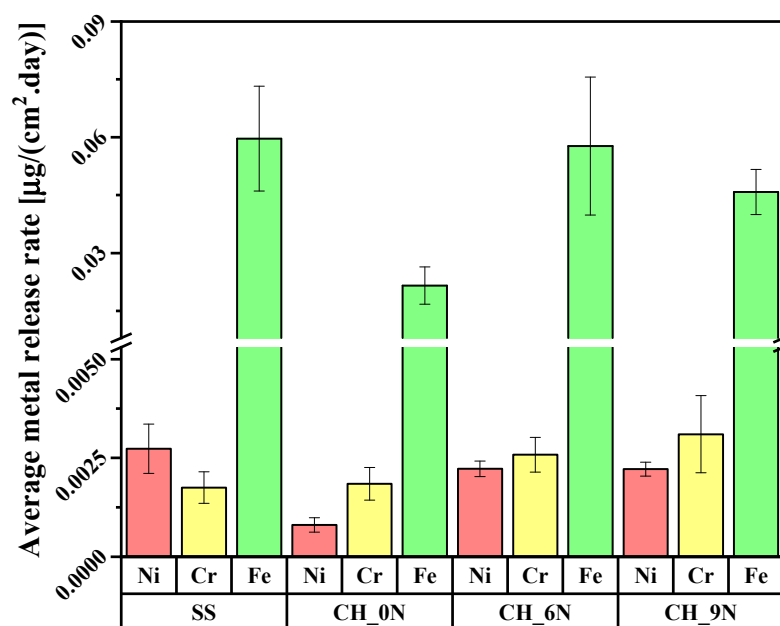
Figure 4. Average Ni, Cr, and Fe release for the uncoated and DLC-coated 316L SS substrates after the 30-day corrosion test in acidic artificial saliva.

3.3. Cytotoxicity Evaluation

After quantifying the concentrations of released metallic ions upon the salivary corrosion, the cytotoxicity effect was evaluated via the MTT assay. The cell viability results for fibroblasts and macrophages and their coculture upon incubation with culture medium conditioned with extracts or saliva are presented in Figure 5. Macrophage primary monocultures were incubated for 5 days, while fibroblast cell line monoculture and their coculture with macrophages were incubated for 6 days. Overall, an analysis of this figure shows that the median MTT values of all groups are above the 70% level [25], suggesting that all materials are noncytotoxic.

3.3.1. Macrophages

Concerning the MTT results from the macrophage monocultures, statistically significant differences were found between saliva and SS ($p < 0.01$), CH_0N ($p < 0.001$), CH_6N ($p < 0.001$), and CH_9N ($p < 0.01$); SS and CH_0N ($p < 0.001$), CH_6N ($p < 0.001$), and CH_9N ($p < 0.001$); and between CH_6N and CH_9N ($p < 0.05$), as presented in Figure 5a.

The SS group shows the lowest cell viability, with statistically significant differences regarding all the other groups of coated samples (Figure 5a). These findings seem to follow the overall reduction in the metal release rates upon coating with the DLC, as presented in Figure 4.

Significant attention has been given to the cytotoxicity of nickel (Ni) [43]. In fact, the International Agency for Research on Cancer (IARC) classifies nickel compounds as carcinogenic to humans (Group I), while metallic nickel is potentially carcinogenic [5].

In a recent study, Loeffler et al. [44] investigated the in vitro inflammatory effects over THP-1 monocytes and macrophages after exposure to separate solutions of Cr(III) and Ni(II) ions with successively higher concentrations (10–500 µM, found in periprosthetic tissues). The authors reported that Cr(III) did not significantly influence the cell viability of both types of cells for the tested concentration range; conversely, Ni(II) ions induced cytotoxic effects that were concentration-dependent. Moreover, low concentrations of bivalent ions were found to trigger the release of inflammatory mediators, especially from macrophages. For Ni(II) solutions with the highest concentrations (100 and 500 µM), however, the reactive oxygen species (ROS) significantly increased in the supernatant compared to the control. ROS are produced by innate immune system cells to deal with pathogens; nonetheless, for

high production, ROS can accumulate and induce oxidative cell stress, leading to oxidation of cellular biomolecules and possibly cell damage or death [44], which may be occurring in this study.
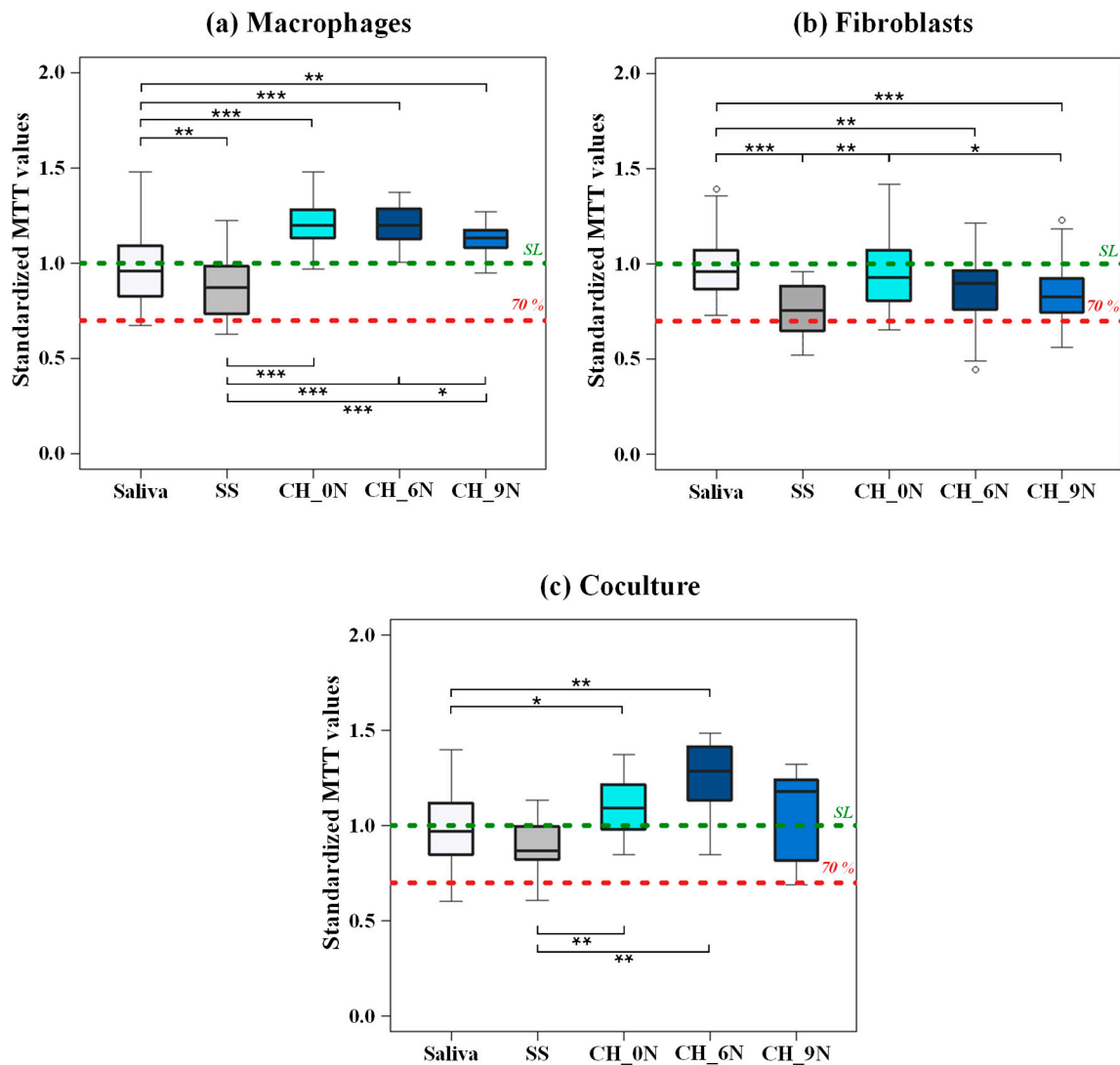

Figure 5. MTT cell viability results of (**a**) macrophages (5 days), (**b**) fibroblasts (6 days), and (**c**) coculture (6 days) after the test in culture medium conditioned with saliva or with extracts from SS, CH_0N, CH_6N, and CH_9N. The MTT values are expressed as a percentage of each mean value of each experimental control. SL: standardization line. 70%: refers to 70% of the control. Statistical significances: * $p < 0.05$; ** $p < 0.01$; and *** $p < 0.001$.

Regarding chromium, it is accepted that its release during corrosion occurs in its trivalent ionic form, despite evidence of the in vivo release of Cr(IV), which is rapidly reduced to Cr(III) in cells [45]. While Cr's toxicity is usually assigned to its hexavalent oxidation state, other researchers pointed out "the potential for Cr(III) to cause toxic, carcinogenic, genotoxic, mutagenic, and epigenetic effects in biological systems" [46]. Nevertheless, Cr average release rates were similar for all tested samples. Thus, the contents of both Ni(II) and Cr(II) ions may help explain the statistically significant differences found between the uncoated and coated SS groups.

Interestingly, standardized MTT average values above the SL line ($y = 1$) were found when macrophages were incubated with the culture medium conditioned using the extracts from the coated samples (CH_0N, CH_6N, and CH_9N), but that was not the case for the saliva group (i.e., macrophages grown with medium conditioned with artificial saliva

without corrosion extracts), Figure 5a. Explaining this result is challenging. One potential justification could be the activation of the macrophages, namely regarding the release of Fe and their fundamental role in vivo [47,48]. Iron is an essential trace metal for living organisms, taking part in multiple vital functions and metabolic pathways, such as oxygen transport throughout the body and DNA synthesis [47,49]. For 19–50-year-old men and women (nonpregnant, not breastfeeding), recommended dietary allowances (RDA) of ~8 and 18 mg/day of Fe were estimated [50], respectively, even though only a portion will be biologically accessible. After absorption in the duodenal mucosa cells via a divalent metal transporter-1 (DMT-1), a strictly regulated and complex homeostasis of this metallic element occurs, in which macrophages play an important role [47,48]. The tight Fe regulation is justified due to the capacity of "free" iron to donate or accept electrons from other molecules and to consequently produce ROS [48,51–53]. This is the case of ferrous Fe(II) ions, which are commonly released during metallic corrosion processes.

Due to the potential cytotoxicity of its ions, Fe does not move freely throughout the body. Instead, it is maintained "captive", either bonded to other molecules (e.g., ferritin) or compounds, and/or kept inside the cells [47,48]. Macrophages are cells from the innate immune system that play a pivotal role in dealing with this metal [47,53]. For instance, specialized spleen and liver macrophages phagocytize damage or senescent red blood cells to collect iron that is found in the heme groups of hemoglobin. Moreover, differently polarized M1 or M2 macrophages can sequestrate or release iron, respectively. M1-like macrophages maximize their ability to retain Fe inside the cells to restrict its availability to pathogens (e.g., during bacterial infections) or under an inflammatory response. Conversely, the fast iron release promoted by M2-like macrophages induces tissue repair and regeneration, angiogenesis, and inflammation resolution [47,48,53].

In the current study, the increased MTT values for macrophages incubated with culture medium conditioned with corrosion extracts from coated samples—when compared to the SL and the saliva group—may be related to their higher activity. According to the abovementioned role in Fe homeostasis they play, macrophages may be importing these ions from the extracts present in the culture medium. A higher activation of the naïve macrophages based upon this factor could explain the increased MTT colorimetric assay values for cultures conditioned with the corrosion extracts [54], whereas the same would not occur for the controls or the saliva group, which do not have such concentration in Fe.

Despite the remarkable ability of macrophages to adapt to external stimuli, a decrease in cell viability was found between the CH_6N and CH_9N groups ($p < 0.05$), Figure 5a. Data suggests an overall decrease trend in cell viability for macrophages cultured with corrosion extracts as follows: CH_0N $\simeq$ CH_6N > CH_9N > SS. Particular attention should be given to macrophages cultured with medium conditioned with the eluates from the uncoated SS, which showed a statistically significant decrease in cell viability, evidencing it is poorer in vitro biocompatibility when compared with the coated samples.

Overall, the best cell viability results obtained for macrophages were obtained for the CH_0N and CH_6N coatings.

3.3.2. Fibroblasts

The statistical analysis of the results from the fibroblast monocultures revealed statistically significant differences between the following groups: saliva and SS ($p < 0.001$), CH_6N ($p < 0.01$) and CH_9N ($p < 0.001$); SS and CH_0N ($p < 0.01$); and CH_0N and CH_9N ($p < 0.05$), Figure 5b.

Generically, the results from the fibroblast monocultures show that all medians were below the SL line. All the studied groups showed a decrease in the median cell viability, in the following order: saliva > CH_0N > CH_6N > CH_9N > SS (Figure 5b). The worst cell viability was obtained for the extracts released from the medical grade 316L SS, whose median is above but quite close to the 70% level. In the frame of the current work, the extracts from SS can still be classified as biocompatible (as expected); however, the carbon-

based coatings were found to significantly increase the overall biocompatibility. Moreover, the extracts from the undoped CH_0N coating showed the best cell viability.

The isolated effect of Ni ions on the viability and number of different types of fibroblasts were studied by other researchers [55]. Accordingly, 50% of cell death and cell viability were found for BALB/3T3 clone A31 fibroblast for Ni ions concentrations of ~0.05 and 0.09 mM/L, respectively [55]. Ni is also capable of actively inducing ROS in intact mammalian cells, which may be the first step of a Ni-mediated ROS mechanism of Ni carcinogenicity [56]. Moreover, Ni was found to reprogram the metabolism of primary human lung fibroblasts and mouse embryonic fibroblasts by strongly repressing mitochondrial fatty acid oxidation, which may contribute to Ni-induced carcinogenicity [57]. Dioxygenases are also inhibited by Ni ions, which can have widespread negative effects on cells, namely concerning DNA repair [58].

The effect of Fe ions in fibroblasts' viability cannot be disregarded as well [59]. In fact, the cytotoxicity to BALB/3T3 with solutions of iron chloride was found to be concentration-dependent, and a synergistic effect with nickel chloride solutions may occur [60]. Additionally, cell membranes can be damaged by iron ions via Fenton and Haber–Weiss reactions due to the production of ROS [52].

In the current work, a combined effect between the three metallic ions in the extracts may influence the overall cell viability of fibroblast monocultures.

3.3.3. Coculture

Finally, statistically significant differences were found for the MTT results of the coculture between the following groups: saliva and CH_0N ($p < 0.05$) and CH_6N ($p < 0.01$); and between SS and CH_0N and CH_6N (both $p < 0.01$), Figure 5c.

The cell viability results confirm that the extracts released from the SS were the least biocompatible, especially compared with both CH_0N and CH_6N (Figure 5c). A higher dispersion was assessed for the results of CH_9N, but the median value was between those of CH_0N and CH_9N. Moreover, all the groups concerning coated samples showed: (i) median MTT values above the SS, as found for isolated monocultures of macrophages; and (ii) nonsignificant differences among them.

The results suggest that the SS extracts decrease cell viability even though the difference between the SS and saliva groups was nonsignificant. The impact of these extracts thus seems to be lower for the coculture when compared with the monocultures. The coculture assays are expected to better mimic the in vivo scenario, in which different types of cells simultaneously interact in a collaborative manner. For instance, fibroblasts can synthesize and release growth factors [61] that can enhance the survival of macrophages, whereas this phagocytic cell type can improve the quality of the culture medium by removing adverse chemical stimuli [62]. Additionally, the cell viability overestimation effect mentioned for macrophages may also be present in the coculture experiment (and not in the fibroblast monoculture). This may help explain the abnormal increase in the median MTT values for the groups of coated samples (CH_0N, CH_6N, and CH_9N). Nonetheless, it was absent for SS, which indicates a poorer in vitro biocompatibility of the 316L medical-grade alloy when uncoated.

As in all in vitro studies, this research work presents some limitations which do not enable absolute extrapolations to more complex real applications of the coated 316L SS, such as orthodontics. On one hand, extracts for the cell viability assays were produced after a 30-day release of metallic ions, while longer contact with the intraoral tissues occurs in the in vivo situations. In fact, standard treatment for dental malocclusion may last for approximately 2 years. Moreover, the cleansing effect of saliva and the possible uptake by oral micro-organisms may limit the cell exposure to metallic ions. On the other hand, additional factors of the intraoral cavity, such as dynamic changes in chemical composition, temperature, and pH, further enhanced by wear mechanisms (e.g., on the bracket/archwire contact) and Microbiologically Induced Corrosion (MIC), can increase metal release from fixed appliances. Nonetheless, the current study showed that the

biocompatibility of medical-grade SS alloys can be further enhanced by using surface functionalization strategies, such as coating with a-C:H-based materials.

Finally, the present research revealed that both the metal release and cell viability do not follow the good results regarding the superior bacterial inhibition properties of coatings with an N-doping level of ~6 at.% [13].

4. Conclusions

In this study, hydrogenated amorphous carbon coatings were successfully modified by nitrogen addition, via reactive magnetron sputtering. Two N doping contents of 6 and 9 at.% were attained.

These low doping levels (<10 at.%) should be an improvement of the coated 316L stainless steel corrosion behavior. Indeed, no microstructural changes, detachments and/or cracking of the coatings were observed upon the 30-day acidic immersion test. The most effective protecting behavior of the SS alloys was found for the undoped CH_0N film, according to the lowest metal release rates obtained.

The cell viability test results showed that all coated samples were biocompatible, since their medians exceeded the 70% level regarding the control. The good biocompatibility of the medical grade 316L SS was further enhanced upon surface modification via carbon materials deposition, with or without N addition.

These findings reinforce the need for simultaneously assessing both the physiochemical and biological properties of materials intended to be used in the medical field.

References

1. Hiromoto, S. Corrosion of Metallic Biomaterials. In *Metals for Biomedical Devices*; Woodhead Publishing: Cambridge, UK, 2019; pp. 131–152, ISBN 978-0-08-102666-3.
2. Eliaz, N. Corrosion of Metallic Biomaterials: A Review. *Materials* **2019**, *12*, 407. [CrossRef] [PubMed]
3. Proffit, W.R.; Fields, H.W.; Sarver, D.M.; Ackerman, J.L. Contemporary Orthodontic Appliances. In *Contemporary Orthodontics*; Elsevier: Amsterdam, The Netherlands, 2012; pp. 347–389, ISBN 978032308317.
4. Fróis, A.; Santos, A.C.; Louro, C.S. Corrosion of Fixed Orthodontic Appliances: Causes, Concerns, and Mitigation Strategies. *Metals* **2023**, *13*, 1955. [CrossRef]
5. IARC (International Agency for Research on Cancer). Nickel and Nickel Compounds. *IARC Monogr. Eval. Carcinog. Risks Hum.* **2011**, *100C*, 169–218. [CrossRef]

6.   Noble, J.; Ahing, S.I.; Karaiskos, N.E.; Wiltshire, W.A. Nickel Allergy and Orthodontics, a Review and Report of Two Cases. *Br. Dent. J.* **2008**, *204*, 297–300. [CrossRef]

7.   Arango, S.; Peláez-Vargas, A.; García, C. Coating and Surface Treatments on Orthodontic Metallic Materials. *Coatings* **2013**, *3*, 1–15. [CrossRef]

8.   Glocker, D.A. Sputter Deposition and Sputtered Coatings for Biomedical Applications. In *Medical Coatings and Deposition Technologies*; Glocker, D., Ranade, S., Eds.; Wiley: Hoboken, NJ, USA, 2016; pp. 531–552, ISBN 978-1-118-03194-0.

9.   Baptista, A.; Silva, F.; Porteiro, J.; Míguez, J.; Pinto, G. Sputtering Physical Vapour Deposition (PVD) Coatings: A Critical Review on Process Improvement and Market Trend Demands. *Coatings* **2018**, *8*, 402. [CrossRef]

10.   Ohgoe, Y.; Hirakuri, K.K.; Saitoh, H.; Nakahigashi, T.; Ohtake, N.; Hirata, A.; Kanda, K.; Hiratsuka, M.; Fukui, Y. Classification of DLC Films in Terms of Biological Response. *Surf. Coat. Technol.* **2012**, *207*, 350–354. [CrossRef]

11.   Malisz, K.; Świeczko-Żurek, B.; Sionkowska, A. Preparation and Characterization of Diamond-like Carbon Coatings for Biomedical Applications—A Review. *Materials* **2023**, *16*, 3420. [CrossRef]

12.   Okpalugo, T.I.T.; Ogwu, A.A. DLC Thin Films for Implantable Medical Devices. In *Thin Film Coatings for Biomaterials and Biomedical Applications*; Elsevier: Amsterdam, The Netherlands, 2016; pp. 261–287, ISBN 978-1-78242-476-5.

13.   Fróis, A.; Francisco, R.; Morais, P.V.; Santos, L.F.; Peres, M.; Lorenz, K.; Santos, A.C.; Louro, C.S. The Influence of Low Nitrogen Doping on Bacterial Adhesion of Sputtered A-C:H Coatings. *Diam. Relat. Mater.* **2024**, *147*, 111309. [CrossRef]

14.   Ferrari, A.C.; Robertson, J. Interpretation of Raman Spectra of Disordered and Amorphous Carbon. *Phys. Rev. B* **2000**, *61*, 14095–14107. [CrossRef]

15.   Robertson, J. Diamond-like Amorphous Carbon. *Mater. Sci. Eng. R Rep.* **2002**, *37*, 129–281. [CrossRef]

16.   *ISO 10271:2001*; Dental Metallic Materials—Corrosion Test Methods. ISO (International Organization for Standardization): Geneva, Switzerland, 2001.

17.   Madamba, D. The Effect of Surface Treatment on Nickel Leaching from Nitinol. Master's Thesis, San Jose State University, San Jose, CA, USA, 2013.

18.   Fróis, A.; Aleixo, A.S.; Evaristo, M.; Santos, A.C.; Louro, C.S. Can A-C:H-Sputtered Coatings Be Extended to Orthodontics? *Coatings* **2021**, *11*, 832. [CrossRef]

19.   ATCC (American Type Culture Collection) NIH/3T3 (ATCC CRL-1658). Available online: https://www.atcc.org/products/crl-1658 (accessed on 27 June 2024).

20.   Santos, A.C.A. Água Trocável Do Pulmão: Contribuição Para o Desenvolvimento de Uma Metodologia Para a Sua Avaliação. Ph.D. Thesis, Universidade de Coimbra, Coimbra, Portugal, 2001.

21.   *ISO 10993-5:2009*; Biological Evaluation of Medical Devices—Part 5: Tests for In Vitro Cytotoxicity. ISO (International Organization for Standardization): Geneva, Switzerland, 2009.

22.   Costa, M.T.; Lenza, M.A.; Gosch, C.S.; Costa, I.; Ribeiro-Dias, F. In Vitro Evaluation of Corrosion and Cytotoxicity of Orthodontic Brackets. *J. Dent. Res.* **2007**, *86*, 441–445. [CrossRef]

23.   Riss, T.L.; Moravec, R.A.; Niles, A.L.; Duellman, S.; Benink, H.A.; Worzella, T.J.; Minor, L. Cell Viability Assays. In *Assay Guidance Manual*; Sittampalam, G.S., Grossman, A., Brimacombe, K., Arkin, M., Auld, D., Austin, C.P., Baell, J., Bejcek, B., Caaveiro, J.M.M., Chung, T.D.Y., et al., Eds.; Eli Lilly & Company and the National Center for Advancing Translational Sciences: Bethesda, MD, USA, 2013; pp. 295–320.

24.   Posit Team. *RStudio: Integrated Development Environment for R. Posit Software*; PBC: Boston, MA, USA, 2023; Available online: http://www.posit.co/ (accessed on 10 November 2024).

25.   Srivastava, G.K.; Alonso-Alonso, M.L.; Fernandez-Bueno, I.; Garcia-Gutierrez, M.T.; Rull, F.; Medina, J.; Coco, R.M.; Pastor, J.C. Comparison between Direct Contact and Extract Exposure Methods for PFO Cytotoxicity Evaluation. *Sci. Rep.* **2018**, *8*, 1425. [CrossRef]

26.   Dalibón, E.L.; Escalada, L.; Simison, S.; Forsich, C.; Heim, D.; Brühl, S.P. Mechanical and Corrosion Behavior of Thick and Soft DLC Coatings. *Surf. Coat. Technol.* **2017**, *312*, 101–109. [CrossRef]

27.   Goldschmidt, H.J. *Interstitial Alloys*; Elsevier: London, UK, 1967; ISBN 9781483200705.

28.   Wenzel, R.N. Resistance of Solid Surfaces to Wetting by Water. *Ind. Eng. Chem.* **1936**, *28*, 988–994. [CrossRef]

29.   Ryan, B.J.; Poduska, K.M. Roughness Effects on Contact Angle Measurements. *Am. J. Phys.* **2008**, *76*, 1074–1077. [CrossRef]

30.   Sun, L.; Guo, P.; Li, X.; Wang, A. Comparative Study on Structure and Wetting Properties of Diamond-like Carbon Films by W and Cu Doping. *Diam. Relat. Mater.* **2017**, *73*, 278–284. [CrossRef]

31.   Cloutier, M.; Harnagea, C.; Hale, P.; Seddiki, O.; Rosei, F.; Mantovani, D. Long-Term Stability of Hydrogenated DLC Coatings: Effects of Aging on the Structural, Chemical and Mechanical Properties. *Diam. Relat. Mater.* **2014**, *48*, 65–72. [CrossRef]

32.   Khun, N.W.; Liu, E.; Zeng, X.T. Corrosion Behavior of Nitrogen Doped Diamond-like Carbon Thin Films in NaCl Solutions. *Corros. Sci.* **2009**, *51*, 2158–2164. [CrossRef]

33.   Borowski, T.; Spychalski, M.; Rożniatowski, K.; Kulikowski, K. Corrosion Resistance of Nitrogen-Doped DLC Coatings Produced in Glow Discharge Conditions on Nitrided Austenitic Steel. *Arch. Metall. Mater.* **2020**, *65*, 1141–1146. [CrossRef]

34.   Marton, M.; Kovalčík, D.; Vojs, M.; Zdravecká, E.; Varga, M.; Michalíková, L.; Veselý, M.; Redhammer, R.; Písečný, P. Electrochemical Corrosion Behavior of Amorphous Carbon Nitride Thin Films. *Vacuum* **2012**, *86*, 696–698. [CrossRef]

35. Sui, J.H.; Zhang, Z.G.; Cai, W. Surface Characteristics and Electrochemical Corrosion Behavior of Fluorinated Diamond-like Carbon (F-DLC) Films on the NiTi Alloys. *Nucl. Instrum. Methods Phys. Res. Sect. B Beam Interact. Mater. At.* **2009**, *267*, 2475–2479. [CrossRef]

36. Ohgoe, Y.; Kobayashi, S.; Ozeki, K.; Aoki, H.; Nakamori, H.; Hirakuri, K.K.; Miyashita, O. Reduction Effect of Nickel Ion Release on a Diamond-like Carbon Film Coated onto an Orthodontic Archwire. *Thin Solid Films* **2006**, *497*, 218–222. [CrossRef]

37. Kobayashi, S.; Ohgoe, Y.; Ozeki, K.; Hirakuri, K.; Aoki, H. Dissolution Effect and Cytotoxicity of Diamond-like Carbon Coatings on Orthodontic Archwires. *J. Mater. Sci. Mater. Med.* **2007**, *18*, 2263–2268. [CrossRef]

38. Li, J.; Zhang, Y.; Qin, Y.; Xiao, B.; Wang, S. Improvement of Cu and Zr Doped Diamond-like Carbon Coatings on Comprehensive Performance of Ni-Ti Alloy Potentially Used in Braided Vascular Stent. *Thin Solid Films* **2023**, *782*, 140020. [CrossRef]

39. Resen, A.M. Surface Modification of Co-Cr-Mo Alloy by Plasma Assisted CVD. *Mater. Today Proc.* **2021**, *42*, 2896–2900. [CrossRef]

40. Hang, R.; Zhang, M.; Ma, S.; Chu, P.K. Biological Response of Endothelial Cells to Diamond-like Carbon-coated NiTi Alloy. *J. Biomed. Mater. Res. Part A* **2012**, *100A*, 496–506. [CrossRef]

41. Ilic, E.; Pardo, A.; Suter, T.; Mischler, S.; Schmutz, P.; Hauert, R. A Methodology for Characterizing the Electrochemical Stability of DLC Coated Interlayers and Interfaces. *Surf. Coat. Technol.* **2019**, *375*, 402–413. [CrossRef]

42. Nilkar, M.; Ghodsi, F.E.; Jafari, S.; Thiry, D.; Snyders, R. Effects of Nitrogen Incorporation on N-Doped DLC Thin Film Electrodes Fabricated by Dielectric Barrier Discharge Plasma: Structural Evolution and Electrochemical Performances. *J. Alloys Compd.* **2021**, *853*, 157298. [CrossRef]

43. Genchi, G.; Carocci, A.; Lauria, G.; Sinicropi, M.S.; Catalano, A. Nickel: Human Health and Environmental Toxicology. *Int. J. Environ. Res. Public Health* **2020**, *17*, 679. [CrossRef] [PubMed]

44. Loeffler, H.; Jonitz-Heincke, A.; Peters, K.; Mueller-Hilke, B.; Fiedler, T.; Bader, R.; Klinder, A. Comparison of Inflammatory Effects in THP-1 Monocytes and Macrophages after Exposure to Metal Ions. *Materials* **2020**, *13*, 1150. [CrossRef] [PubMed]

45. Merritt, K.; Brown, S.A. Release of Hexavalent Chromium from Corrosion of Stainless Steel and Cobalt—Chromium Alloys. *J. Biomed. Mater. Res.* **1995**, *29*, 627–633. [CrossRef] [PubMed]

46. Costa, M.; Murphy, A. Overview of Chromium(III) Toxicology. In *The Nutritional Biochemistry of Chromium (III)*; Elsevier: Amsterdam, The Netherlands, 2019; pp. 341–359, ISBN 978-0-444-64121-2.

47. Jung, M.; Mertens, C.; Brüne, B. Macrophage Iron Homeostasis and Polarization in the Context of Cancer. *Immunobiology* **2015**, *220*, 295–304. [CrossRef]

48. Soares, M.P.; Hamza, I. Macrophages and Iron Metabolism. *Immunity* **2016**, *44*, 492–504. [CrossRef]

49. World Health Organization. Guidelines for Drinking-Water Quality: Fourth Edition Incorporating the First and Second Addenda. 2022. Available online: https://iris.who.int/bitstream/handle/10665/352532/9789240045064-eng.pdf (accessed on 10 November 2024).

50. National Institute of Health—Office of Dietary Supplements Iron. Available online: https://ods.od.nih.gov/factsheets/Iron-HealthProfessional/#h6 (accessed on 28 July 2024).

51. Kaplan, J.; Ward, D.M. The Essential Nature of Iron Usage and Regulation. *Curr. Biol.* **2013**, *23*, R642–R646. [CrossRef]

52. Eid, R.; Arab, N.T.T.; Greenwood, M.T. Iron Mediated Toxicity and Programmed Cell Death: A Review and a Re-Examination of Existing Paradigms. *Biochim. Biophys. Acta-Mol. Cell Res.* **2017**, *1864*, 399–430. [CrossRef]

53. Behmoaras, J. The Versatile Biochemistry of Iron in Macrophage Effector Functions. *FEBS J.* **2021**, *288*, 6972–6989. [CrossRef]

54. Pozzolini, M.; Scarfì, S.; Benatti, U.; Giovine, M. Interference in MTT Cell Viability Assay in Activated Macrophage Cell Line. *Anal. Biochem.* **2003**, *313*, 338–341. [CrossRef]

55. Taira, M.; Toguchi, M.S.; Hamada, Y.; Takahashi, J.; Itou, R.; Toyosawa, S.; Ijyuin, N.; Okazaki, M. Studies on Cytotoxic Effect of Nickel Ions on Three Cultured Fibroblasts. *J. Mater. Sci. Mater. Med.* **2001**, *12*, 373–376. [CrossRef]

56. Terpiłowska, S.; Siwicka-Gieroba, D.; Siwicki, A.K. Cytotoxicity of Iron (III), Molybdenum (III), and Their Mixtures in BALB/3T3 and HepG2 Cells. *J. Vet. Res.* **2018**, *62*, 527–533. [CrossRef] [PubMed]

57. Huang, X.; Zhuang, Z.; Frenkel, K.; Klein, C.B.; Costa, M. The Role of Nickel and Nickel-Mediated Reactive Oxygen Species in the Mechanism of Nickel Carcinogenesis. *Environ. Health Perspect.* **1994**, *102*, 281. [CrossRef] [PubMed]

58. Uppala, R.; McKinney, R.W.; Brant, K.A.; Fabisiak, J.P.; Goetzman, E.S. Nickel Inhibits Mitochondrial Fatty Acid Oxidation. *Biochem. Biophys. Res. Commun.* **2015**, *463*, 806–810. [CrossRef] [PubMed]

59. Chen, H.; Giri, N.C.; Zhang, R.; Yamane, K.; Zhang, Y.; Maroney, M.; Costa, M. Nickel Ions Inhibit Histone Demethylase JMJD1A and DNA Repair Enzyme ABH2 by Replacing the Ferrous Iron in the Catalytic Centers. *J. Biol. Chem.* **2010**, *285*, 7374–7383. [CrossRef] [PubMed]

60. Terpiłowska, S.; Siwicka-Gieroba, D.; Krzysztof Siwicki, A. Cell Viability in Normal Fibroblasts and Liver Cancer Cells after Treatment with Iron (III), Nickel (II), and Their Mixture. *J. Vet. Res.* **2018**, *62*, 535–542. [CrossRef]

61. Buechler, M.B.; Fu, W.; Turley, S.J. Fibroblast-Macrophage Reciprocal Interactions in Health, Fibrosis, and Cancer. *Immunity* **2021**, *54*, 903–915. [CrossRef]

62. Witherel, C.E.; Abebayehu, D.; Barker, T.H.; Spiller, K.L. Macrophage and Fibroblast Interactions in Biomaterial-Mediated Fibrosis. *Adv. Healthc. Mater.* **2019**, *8*, 1–16. [CrossRef]